6
DFT studies and Gas Sensor Modelling

In this chapter, we explore the application of density functional theory (DFT) calculations to investigate the adsorption mechanisms of NO_2 gas molecules on the surfaces of MoS_2 and SnS_2 flakes grown using CVD. The study examines the impact of nitrogen plasma treatment and surface decoration with silver nanoparticles (Ag NPs) on the adsorption energy of NO_2 on MoS_2 surfaces. Additionally, electronic structure calculations of vertically aligned SnS_2 flakes and nitrogen plasma-treated SnS_2 flakes are presented. DFT computations reveal that sulfur vacancy defects on the surface significantly influence NO_2 detection by transitioning the adsorption mechanism from physisorption to chemisorption. The chapter also delves into the adsorption kinetics of NO_2 gas on SnS_2 nanoflake-based chemiresistor sensors, utilizing the Lee and Strano model. This model effectively describes the sensor's response curves and enables the extraction of the irreversible reaction rate for different NO_2 concentrations. Through these analyses, the interplay between surface modifications and NO_2 detection efficiency is comprehensively addressed.

6.1 Requirement of Theoretical Investigations of NO_2 Adsorption

A popular quantum computer modelling method for examining the electronic structure of many-body systems in physics, chemistry, and materials science is called density functional theory, or DFT. The fundamental Hohenberg-Kohn theorems were first presented by Pierre Hohenberg and Walter Kohn in 1964. The first theorem showed that the electron density function $\rho_0(x, y, z)$, which depends on just three variables, may uniquely identify the ground-state energy, wave function, and other electronic features for systems with a non-degenerate fundamental ground state. The ground-state energy might be represented as a functional, $E_0 = E[\rho_0]$, according to the second theorem [Levine, 2014; Sholl et al., 2022]. However, at first, only non-degenerate ground states were covered by the Hohenberg-Kohn theorems. Mel Levy and John P. Perdew expanded the theorem's application in 1967 by including systems with degenerate ground states[Levine, 2014; Sholl et al., 2022].

In addition to experimental investigations, theoretical research has significantly advanced the development of gas-sensing technologies and the prediction of the sensing characteristics of potential materials[Cohen et al., 2012]. Density functional theory (DFT) is a prominent theoretical approach that consistently demonstrates efficiency in terms of time, effort, and cost [Agrawal et al., 2021; Cohen et al., 2012]. DFT provides a comprehensive and precise explanation of the underlying mechanisms occurring between sensing devices and gas analytes [Jones, 2015]. Key features of DFT include the understanding of fundamental interactions between sensing materials and gas analytes, as well as pre-calculations of charge transfers. These characteristics facilitate the exploration of chemical and physical adsorption of gas analytes, theoretical assessments of composites and anchored nanoparticles, and the effects of noble metal and other material functionalization on MoS_2 and SnS_2. For instance, Wenli Li *et al.,* prepared few-layer MoS_2 nanosheets (FLMN) via mechanical exfoliation and coated them onto a substrate with interdigital electrodes for room-temperature NO_2 detection [Li et al., 2019a]. First-principles calculations based on DFT confirmed that the ultrafast recovery behavior is attributed to the weak van der Waals interactions between NO_2 and the MoS_2 surface.

Since the significant role of defects in enhancing sensing properties, the development of sensing materials with defective morphologies is crucial [Kumar et al., 2024b]. In this context, an NO_2 gas sensor was fabricated using edge-enriched and mixed in-plane MoS_2 flakes, which exhibited a rapid response time (8.5 s) and a response of approximately 10.36% to 10 ppm of NO_2 at room temperature. However, the sensor did not achieve complete recovery due to the high adsorption energy of NO_2 gas molecules on the sensor surface (-0.276 eV), as calculated by

DFT[Agrawal et al., 2018]. Additionally, Wang *et al.,* investigated the electronic properties and adsorption behavior of Pd and Rh-functionalized Se-vacancy $MoSe_2$ using DFT, focusing on four gases: SOF_2, SO_2F_2, SO_2, and H_2S. The Se vacancies in $MoSe_2$, along with Rh and Pd transition metal atoms, formed strong chemical bonds (E_b = -3.950 eV and -4.780 eV, respectively). Both Rh and Pd-doped structures exhibited excellent adsorption characteristics for SO_2, although their adsorption capabilities varied for the four gases (Pd: SO_2 > H_2S > SOF_2 > SOF_2; Rh: SO_2 > SOF_2 > SOF_2 > H_2S)[Sang et al., 2022].

The decoration of noble metal nanoparticles is a common strategy to improve the selectivity of chemical sensor arrays utilizing 2D semiconductor materials, such as MoS_2. Kim *et al.,* reported that 2D MoS_2 nanoflakes decorated with noble metals exhibited significant gas sensing selectivity [Kim et al., 2023]. First-principles DFT simulations were used to investigate the effect of noble metal nanoparticle decoration affects selectivity changes, a unique phenomenon resulting from the distinctive structure and highly active edge sites of 2D materials. For example, Ni was doped into MoS_2 nanosheets at concentrations of 3, 5, and 7 atomic percent for room-temperature NO_2 sensing. The increased edge active sites in Ni-incorporated sensors were responsible for the enhanced sensing performance. In pristine MoS_2, only a limited number of active adsorption sites were available for gas adsorption. However, as Ni content increased, more edges and active centers were generated within MoS_2, leading to a 115% improvement in response to 200 ppm of NO_2 at room temperature. DFT studies indicated that the bandgap of the MoS_2 film decreased from 1.73 eV to 1.44 eV after Ni doping, facilitating easier electron transfer from the valence band to the conduction band. Furthermore, the calculations demonstrated that Ni loses electrons while MoS_2 gains them, significantly tuning the sensor's response and chemical activity [Bharathi et al., 2022]. Additionally, Zange Li *et al.*, utilized DFT calculations to modify the SnS_2 monolayer through N, P, Ge, and Se doping, investigating the adsorption properties and gas-sensing mechanisms of each doped SnS_2 variant. Their analysis of adsorption energy, charge density differences, band structure, and recovery times revealed that Ge and Se doping negatively impacted H_2S detection, while N and P doping effectively enhanced the interaction between SnS_2 and H_2S, maintaining physisorption with adsorption energies of -0.60 eV and -0.64 eV, respectively [Li et al., 2024]. In the realm of nanotubes, 2D, and 3D porous nanomaterials, Pd is a widely utilized transition metal for surface decoration. DFT calculations have been employed to assess the sensitivity of bare $MoSe_2$ and Pd-$MoSe_2$ against SO_2F_2 and SOF_2, revealing that Pd doping significantly enhances the gas response of $MoSe_2$[Qian et al., 2019].

6.2 Vienna Ab initio Simulation Package (VASP)

The Vienna Ab initio Simulation Package (VASP) is a software suite designed for quantum mechanical modeling from first principles. It employs methods such as the projected augmented wave (PAW) pseudopotentials or Vanderbilt pseudopotentials combined with a plane wave basis set[Panigrahi et al., 2019]. While its core methodology is based on density functional theory (DFT), VASP also supports post-DFT corrections, including hybrid functionals that integrate DFT with Hartree-Fock exchange, such as HSE [Heyd et al., 2003], PBE0 [Perdew et al., 1996], and B3LYP[Kim et al., 1994]. Additionally, it incorporates advanced techniques like many-body perturbation theory (the GW method) and dynamical electronic correlations using the random phase approximation.

Originally derived from code developed by Mike Payne at MIT, which also served as the foundation for CASTEP, VASP was transferred to the University of Vienna in July 1989 under the direction of Jürgen Hafner. The main program was subsequently developed by Jürgen Furthmüller and Georg Kresse, with Kresse currently leading its development. Recent enhancements include extending methods commonly used in molecular quantum chemistry, such as MP2, to periodic systems. Today, VASP is utilized by over 1,400 academic and industrial research groups worldwide under software license agreements with the University of Vienna.

6.3 Computational Method

6.3.1. Ag NPs anchored-nitrogen plasma treated MoS_2 (Ag-N-MoS_2) flakes

The electronic structure calculations reported in this study were conducted using the Vienna Ab initio Simulation Package (VASP) [Sun et al., 2003]. Ionic relaxation was conducted using the projector augmented wave (PAW) [Blöchl, 1994] method of density functional theory, and all atoms were assumed to have Perdew−Burke−Ernzerhof (PBE) pseudopotentials [Perdew et al., 1998]. Due to inadequacy of Generalized Gradient Approximation (GGA) to incorporate the Van-der Waal's (vDW) interactions, Grimme's DFT-D3 dispersion corrections were used in all calculations. The structural parameters of crystalline MoS_2 were obtained from the Materials Project database version 2023.11.1. The cell parameters of this structure were a= 3.19 Å, b= 3.19 Å, and c= 13.37 Å, with $\alpha = 90°$, $\beta = 90°$, and $\gamma = 120°$. For gas adsorption, a supercell of 4 × 4 × 1 MoS_2 monolayer was constructed, with a 20 Å vacuum maintained between two consecutive layers. K-point sampling was conducted for plane waves using a 4 × 4 × 1 grid with a 400-eV cutoff energy. We employed the conjugate gradient algorithm to relax the geometries, and all calculations were spin-polarized.

6.3.2. Vertically Aligned SnS2 (VA-SnS_2) flakes

The electronic structure calculations were done by Vianna Ab-Initio Simulation Package (VASP) package [Hafner, 2008] and optimised structures are visualised by VESTA software [Momma et al., 2011]. Projected Augmented Wave (PAW) method of density functional theory is used for ionic relaxation due to its reasonable accuracy and computational efficiency about to exhibit the core valance electronic interactions [Kresse et al., 1996]. Perdew-Burke-Ernzerhof (PBE) pseudopotentials are used for all the atoms. 3x3x1 supercell of SnS_2 monolayer is constructed for gas adsorption and vacuum layer of 20 Å is maintained between two consecutive layers. 8x8x1 grid is used for K-points sampling with 400 eV cut-off energy for plane waves. To investigate the adsorption of different gases on the monolayer, each gas molecule was kept 3.5 Å above the surface. All calculations are spin polarised and Conjugate gradient algorithm is employed for relaxing the geometry. All the electronic structure calculations reported here are 0 K calculations.

6.3.3. Vacancy-Assisted Vertically Aligned SnS2 (Vs-SnS_2) flakes

Vianna Ab-Initio Simulation Package (VASP) [Sun et al., 2003] was used for performing the electronic structure calculations reported in the present work. Projected Augmented Wave (PAW) [Blöchl, 1994] method of density functional theory was used for ionic relaxation and Perdew-Bruke-Ernzerhof (PBE)[Perdew et al., 1998] pseudopotentials were used for all atoms. The structural parameters of crystalline SnS_2 were received from the Materials Project for SnS_2 (mp-1170) from database version v2022.10.28. This structure exhibits hexagonal lattice system and $P\bar{3}m1$ space group with cell parameters: a=3.67Å, b=3.67Å and c=6.23Å with $\alpha = 90^0$, $\beta = 90^0$, $\gamma=120^0$. A supercell of 3x3x1 of SnS_2 monolayer was constructed for gas adsorption maintaining 20 Å vacuum between two consecutive layers. 8x8x1 grid was used for K-points sampling with 400 eV cut-off energy for plane waves. All calculations were done by keeping NO_2 at a distance of 3.5 Å above the monolayer surface. All calculations were spin polarized and conjugate gradient algorithm was employed for relaxing the geometries.

6.4 Result and Discussion

6.4.1. Adsorption properties of Ag NPs anchored-nitrogen plasma treated MoS_2 (Ag-N-MoS_2) flakes

To model the present experiments, three different functionalized MoS_2 monolayers were constructed to investigate the NO_2 gas adsorption properties. The initial system studied was pristine MoS_2 and rest of the systems were nitrogen-doped MoS_2 (N-MoS_2) and Ag-functionalized nitrogen-doped MoS_2 (Ag-N-MoS_2), which will establish the effectiveness of N_2 plasma exposure and silver NP functionalization. These structures were fully optimized before optimizing the gas adsorbed surfaces. The adsorption energy (E_{ad}) of the gas with respect to the surface is defined as,

$$E_{ad} = E_{MoS2+NO2} - E_{MoS2} - E_{NO2} \tag{6.1}$$

Where, the total energy of the surface-gas system is denoted as $E_{MoS2+NO2}$, E_{MoS2} and E_{NO2} are the energies of the surface and gas molecule, respectively.

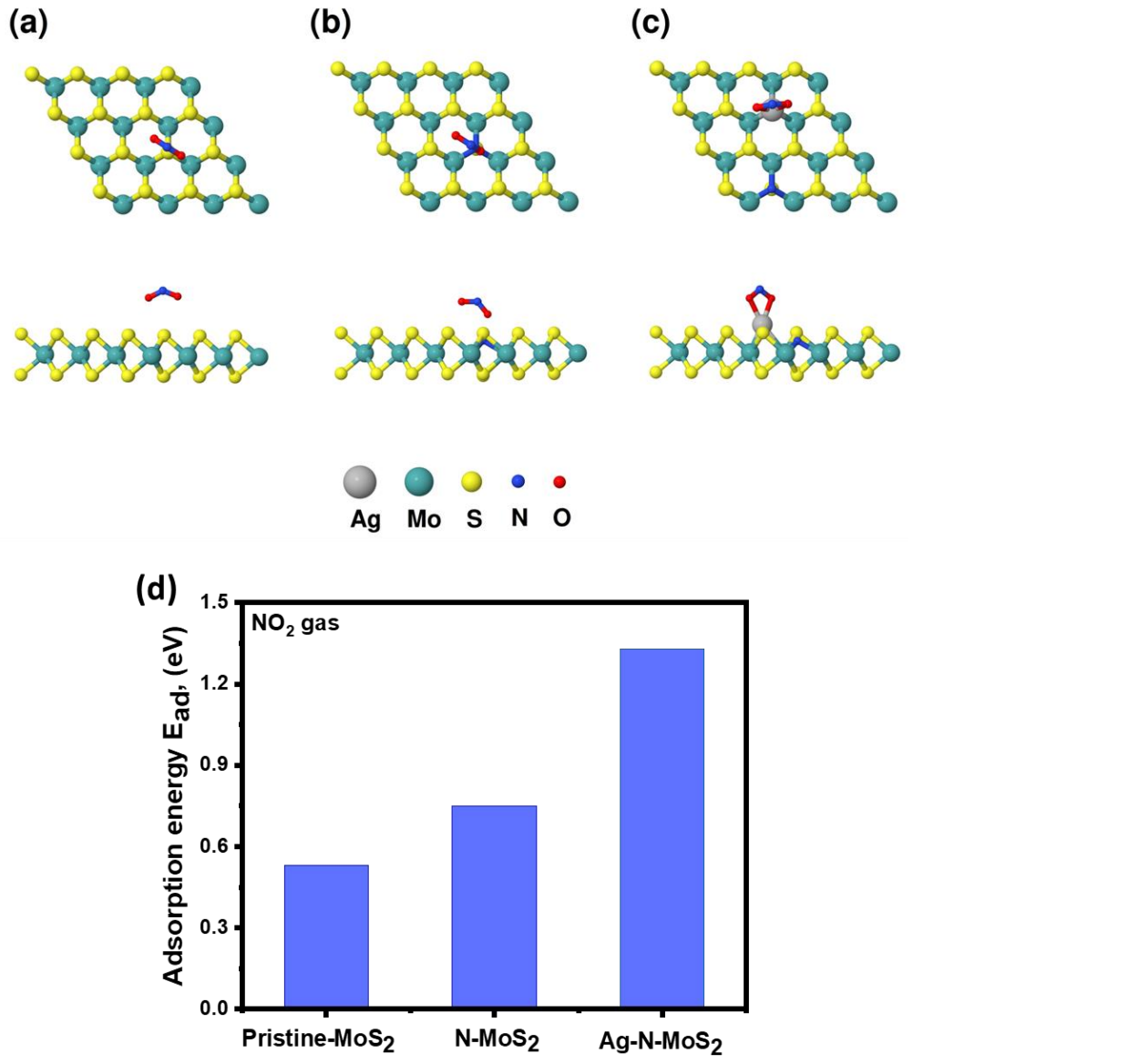


Figure 6.1: The top and side views of NO_2 gas adsorption on the (a) pristine MoS_2 (b) N-MoS_2 and (c) Ag decorated N-MoS_2, and (d) Histogram of adsorption energy pristine MoS_2, N-MoS_2, Ag decorated N-MoS_2, for NO_2 gas.

In the pristine case, a weak van-der Waals interaction between the MoS_2 surface and NO_2 gas was observed, with the lowest adsorption energy of -0.53 eV, suggesting physisorption of gas molecule over the surface, as depicted in Figure 6.1 (a). The relatively low adsorption capacity of pristine MoS_2 to adsorb NO_2 gas has been extensively studied in previous studies]. The material properties, specifically adsorption of the MoS_2 monolayer can be drastically improved by nitrogen doping or functionalizing the material with transition metals through surface modulation. The plasma exposure duration of the MoS_2 surface is a determining factor in the extent of nitrogen doping. The current study examines plasma exposure for a maximum of 8 minutes, which results in a 2-3% atomic nitrogen content of the material. For the theoretical study, the supercell was designed to replicate the effects of nitrogen doping after an 8-minute exposure of N_2 plasma by incorporating a single nitrogen atom into the 4x4x1 MoS_2 monolayer surface. The resultant NO_2 adsorption energy of -0.75 eV was observed. Further, bond lengths between the nitrogen and oxygen atoms in NO_2 gas molecule becomes unequal and, in turn, symmetry is broken (see table 6.1) through the oxygen atom leaning towards the surface nitrogen atom as illustrated in Figure 6.1 (b), resulting $d_{O\text{-}N}$(surface) = 2.06 Å, which suggests a dominant non-bonding interaction. Silver decorated nitrogen doped MoS_2 monolayer increases NO_2 adsorption energy further to -1.33 eV. Figure 6.1 (c) illustrates the adsorption geometry. The presence of two oxygen atoms of NO_2 molecule over the silver atom with an Ag-O bond length of 2.32 Å suggests the existence of robust covalent interactions between the gas molecule and the silver-decorated nitrogen-doped MoS_2 surface.

Table 6.1: Adsorption energies of NO2 gas over different surface systems. The structural changes in configurations are given by bond lengths and bond angles of the constituent elements

System	Adsorption energy (E_{ad}/eV)	After adsorption of NO_2 molecule	
		Bond length (Å)	Angles (degrees)
Gas molecule	-	dN-O = 1.21	O-N-O = 133.3
(b) Pristine MoS_2	-0.53	dN-O = 1.22 dMo-O = 2.41 dO-S = 3.16	O-N-O = 132.1
(c) Nitrogen doped MoS_2 (N- MoS_2)	-0.75	dN-O = 1.21 (away from surface) dN-O = 1.25 (towards surface) dMo-O = 2.41 dO-N(surface) = 2.06	O-N-O = 129.0 N-O-N = 131.4
(d) Silver decorated N-MoS_2 (Ag-N- MoS_2)	-1.33	dN-O = 1.27 dAg-O = 2.32 dAg-Mo = 2.81 dMo-S = 2.42	O-N-O = 113.7 Mo-O-N = 95.9 Mo-Ag-Mo = 67.9

6.4.2. Adsorption properties of Vertically Aligned SnS_2 (VA-SnS_2) flakes

The adsorption properties of NO_2 gas on vertically aligned SnS_2 were studied to identify the most favourable configuration and interaction mechanism. The adsorption energy was calculated using the equation:

$$E_{ads} = E_{[SnS2+NO2]} - E_{[SnS2]} - E_{[NO2]} \quad (6.2)$$

Where, $E_{[SnS2+NO2]}$, $E_{[SnS2]}$, and $E_{[NO2]}$ represent the energies of gas adsorbed system, isolated SnS_2 surface and isolated gas molecules, respectively.

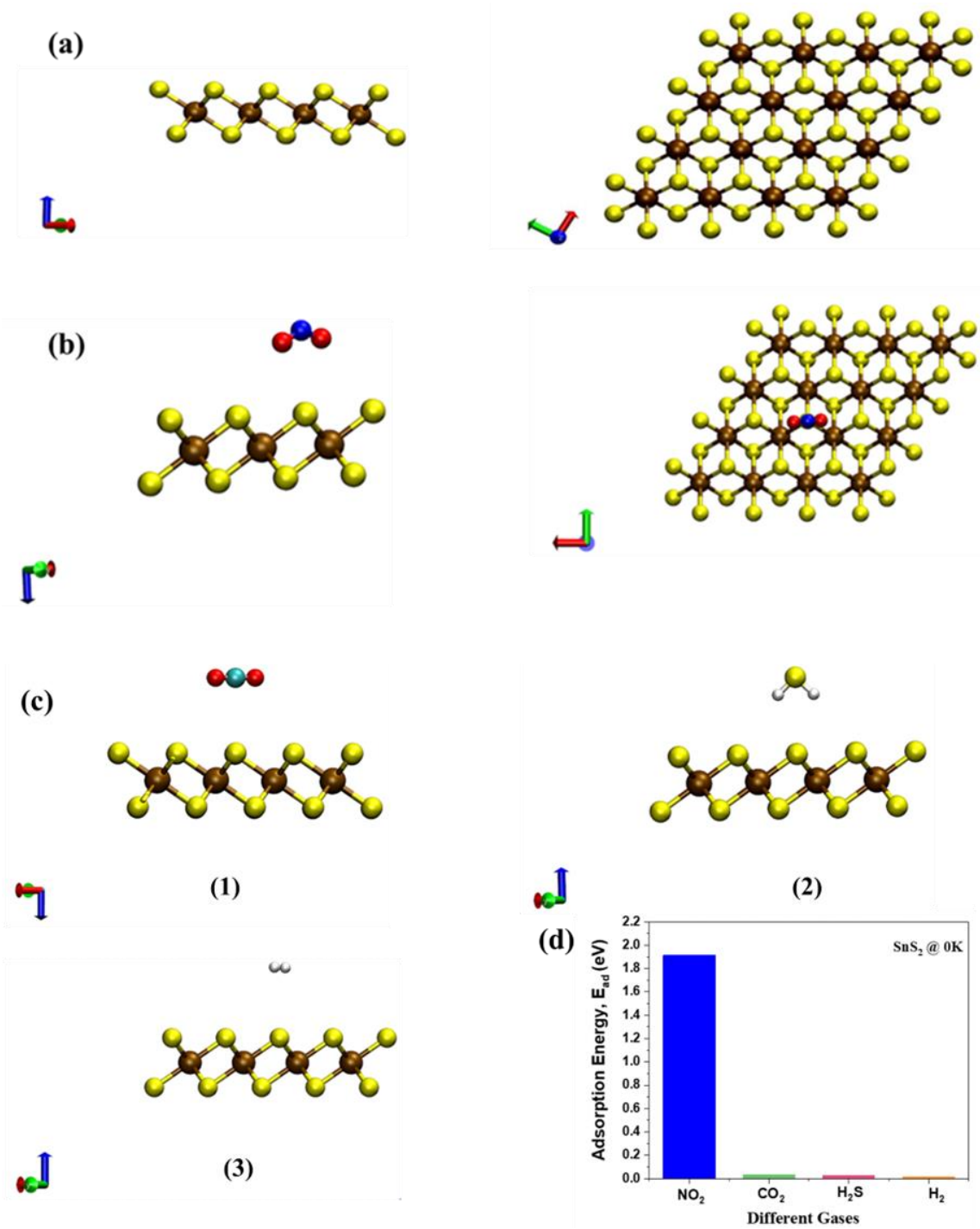


Figure 6.2: (a) The top and side view of a unit cell of monolayer SnS_2, (b) Optimized N atom of NO_2 molecule is adsorbed onto the surfaces of SnS_2 top and side view, (c) Other gases CO_2, H_2S and H_2 kept similar fashion giving optimized structures (1)- (3), and (d) Histogram of adsorption energy for NO_2, CO_2, H_2S and H_2 gas.

After structural optimization, the NO_2 molecule achieved a favorable configuration toward the SnS_2 adsorption surface, as shown in Figure 6.2. The results revealed that NO_2 exhibits the highest binding affinity to the SnS_2 monolayer with an adsorption energy of 1.91 eV, as summarized in Table 6.2. This binding energy is consistent with similar studies on Al-doped SnS_2 monolayers, demonstrating a strong interaction between NO_2 and SnS_2 [Qu et al., 2020]. Structural changes in the NO_2 molecule were evident upon adsorption. The N–O bond length decreased, and the O–N–O bond angle increased significantly by 38.5 degrees at the equilibrium geometry, indicating a substantial structural rearrangement. In contrast, no notable geometric changes were observed for other gases adsorbed on SnS_2, suggesting a unique interaction between NO_2 and the SnS_2 surface. Charge transfer analysis, performed using the Density-Derived Electrostatic and Chemical (DDEC) method, highlighted a significant charge transfer from the NO_2 molecule to the SnS_2 surface compared to other gases. This indicates that the interaction between NO_2 and SnS_2 has a pronounced ionic character, further emphasizing the strong binding affinity of NO_2. The interaction between the vertically aligned SnS_2 and NO_2 was thus confirmed to be highly favorable, with structural and electronic changes supporting its potential for gas-sensing applications.

Table 6.2: Adsorption energy and equilibrium distance along with charge transfer of the developed adsorption systems.

System	Adsorption Energy (eV)	Adsorption length (Å)	Charge Transfer (e)
SnS_2-NO_2	1.914	3.96	-0.04851
SnS_2-CO_2	0.032	4.15	0.00001
SnS_2-H_2S	0.025	4.20	0.00297
SnS_2-H_2	0.016	4.23	-0.00117

6.4.3. Adsorption properties of Vacancy-Assisted Vertically Aligned SnS_2 (Vs-SnS_2) flakes

We subsequently investigate the adsorption properties of NO_2 on vacancy assisted SnS_2 monolayers, focusing on adsorption energy, and charge transfer. The analysis is conducted based on the adsorption structure with the lowest energy configuration. To ensure that the global energy minimum is accurately identified and not confused with a local energy minimum, various adsorption sites and orientations are considered and optimized, as illustrated in Figure 6.3. Three types of supercells were constructed from pristine structure containing one vacant site (I), two conjugate vacant sites (II) and N_2 doped monolayer with one vacant site (III) i.e., one vacancy is replaced by a Nitrogen atom. All three structures were fully optimized before gas-surface calculations. The adsorption energies were calculated by

$$E_{ads} = - [E_{[SnS2\ monolayer+gas]} - E_{[SnS2\ monolayer]} - E_{[NO2]}] \quad (6.3)$$

Where, $E_{[SnS2\ monolayer\ +\ gas]}$, $E_{[SnS2\ monolayer]}$, and $E_{[NO2]}$ represent the energies of gas adsorbed system, isolated SnS_2 surface and isolated gas molecule, respectively. Gas-surface calculations were done by keeping NO_2 above the S vacant sites in all-mentioned structures. The optimized structures are visualized by VESTA[Momma et al., 2008] and JMOL [Hanson, 2010] packages and the relevant energies were computed.

Among all optimized structures, maximum adsorption energy was observed i.e., 2.19 eV with case (I) relative to other systems. This adsorption energy value is greater than NO_2 adsorption

energy with pristine sample (1.91 eV) as previously reported.[Kumar et al., 2022] In the above experiments, 50 ppm adsorption response at 120 °C showed significantly higher response with N12 sample over the pristine (N0) case. NO_2 molecule was chemisorbed on the surface forming strong covalent bond between Sn and O (bond length 1.17Å), in agreement with previously reported theoretical calculations by Rumeng Zhao et al.,[Zhao et al., 2017a] Case (II) has the lowest NO_2 adsorption energy (0.36 eV) whereas Case (III) depicts the intermediate adsorption energy (1.81 eV) as NO_2 binds by weak interactions with the surface. This is in consistent with the significant increase in adsorption of NO_2 gas as depicted by above experiments due to formation of single surface S vacancies up to certain N_2 plasma exposure time i.e., 12 min (N12 sample) and then decreasing after exposing for 16 min (N16 sample) as these vacant sites getting significantly occupied by Nitrogen (Figure 6.4 (a)). We computed the molecule-surface binding energies to evaluate the dispersion forces in order to comprehend the selectivity of Vs_SnS_2 (N12) towards NO_2 gas (Figure 6.4 (b-d)). An additional calculation was carried out for each case keeping gas molecule away from the vacant site above the surface resulting comparatively much lower adsorption energy of NO_2 gas (see Table 6.3).

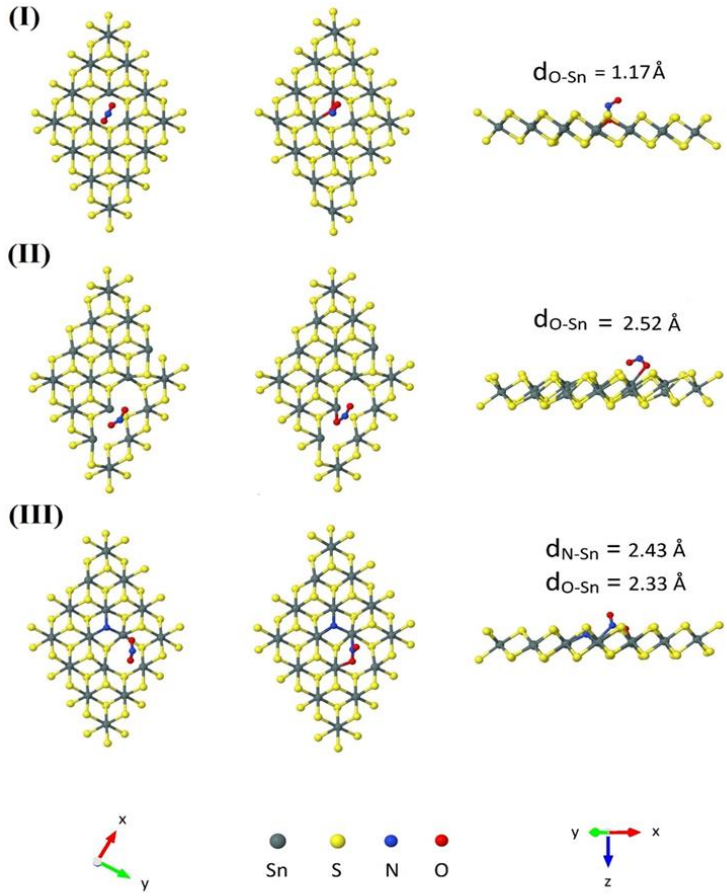


Figure 6.3: Computational model geometries of gas surface system. (a) Initial and optimized structures (from top and side view) of gas-monolayer adsorption system with NO_2 above the sulfur vacant sites with supercell containing single vacant site (I), (b) conjugated double vacant sites (II), and (c) Nitrogen doped single vacant site (III).

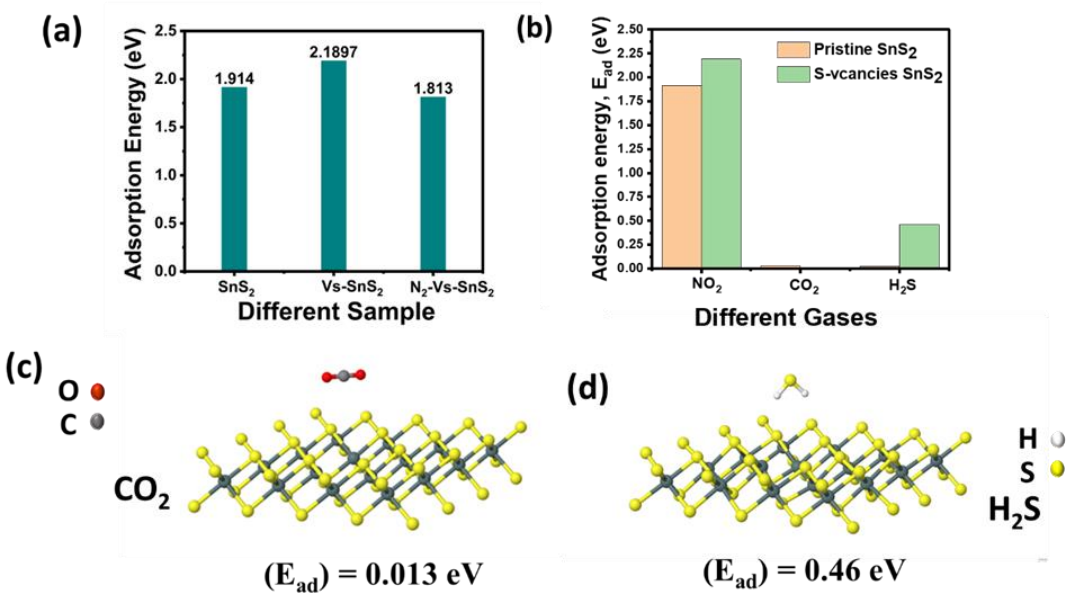


Figure 6.4: (a) Histogram of adsorption energy for pristine (SnS_2), structure containing sulfur vacant site (Vs-SnS_2) and Nitrogen doped monolayer with sulfur vacant site(N_2-Vs-SnS_2), (b) Histogram of adsorption energy for NO_2, CO_2, and H_2S gas, and optimized structures of other gases (c) CO_2, and (d) H_2S.

Table 6.3: Calculated gas adsorption energies of the gas adsorbed over SnS_2 surface

System	Gas adsorption energy (eV)	
	NO_2 on top of Vacancy	NO_2 away from Vacancy
Case I	2.19	0.48
Case II	0.36	0.047
Case III	1.813	-0.0017

6.5 Gas sensor modelling

6.5.1. Gas adsorption-desorption kinetics in 2D material

Adsorption and desorption are vital processes in gas sensing mechanisms, governing how gas molecules interact with sensor materials and determining key performance metrics. In solid-state sensors, these processes influence sensitivity, response time, and recovery, which are essential for effective gas detection and continuous monitoring. Efficient adsorption enables the detection of low concentrations of target gases, while rapid desorption ensures the sensor can quickly return to its baseline state for real-time analysis. In 2D materials, adsorption-desorption dynamics play a pivotal role in defining the reversibility of the sensor's reactions, which is critical for applications requiring repeated use and accurate detection. Kinetic studies of these processes offer valuable insights into gas-surface interactions, impacting the sensor's selectivity and response. For carbon nanotube-based sensors, adsorption dynamics can be modeled using continuum site balance equations and mass action models, revealing both reversible and irreversible binding mechanisms. Irreversible adsorption shows a response time that inversely scales with analyte concentration, where detection is theoretically possible at any nonzero concentration but with longer transduction times for lower concentrations. In contrast, reversible sensors exhibit a fixed detection limit independent of geometry, with a response time that stabilizes at zero analyte concentration. A straightforward analytical test can distinguish these

mechanisms from transient response data, where consistent surface rate constants for irreversible components were identified across various sensor designs and analytes.

Benchmarking sensor responses and comparing the performance of different sensor types require careful consideration, particularly due to the distinct dynamics of reversible and irreversible adsorption mechanisms. Reversible gas sensors establish steady-state signals that correlate with analyte concentration, whereas carbon nanotube-based sensors often exhibit partially irreversible molecular binding for many analytes. This property enables the detection of extremely low analyte concentrations through integral trapping on the sensor surface. However, the presence of irreversible binding sites introduces a tradeoff between detection sensitivity and transduction time, as removing the analyte does not fully regenerate the sensor within the original transduction time scale. The Lee and Strano model provide a mathematical framework to analyse these dynamics, simplifying the interactions between gas molecules and sensor surfaces[Lee et al., 2005]. This model derives critical parameters, such as the adsorption rate constant (k_{ads}) and desorption rate constant (k_{des}), to quantify the interaction kinetics.

In the case of irreversible adsorption, the sensor response cannot be restored within the initial transduction time simply by removing the gas-phase analyte, necessitating alternative regeneration methods. The sensor array under consideration comprises a SnS_2 surface with a fixed number of adsorption sites (Tθ), which corresponds to the total accessible area available for analyte binding. These sites are divided into unoccupied (θ) and occupied (Aθ) categories. The analyte molecule (A), present in the gas phase at a constant concentration (C_a), reacts with an unoccupied site through a surface reaction:

$$\theta\ (sur) + A(g) \rightarrow A\theta(sur) \tag{6.4}$$

In this case, g and sur stand for gas phase and surface bound species, respectively, while k is the forward rate constant. The sensor surface has a conserved number of sites on the surface of SnS_2 sensor.

$$\theta(sur) + A\theta(sur) = T\theta\ (sur) \tag{6.5}$$

In this model, Tθ remains constant, determined by the sensor's accessible surface area. The sensor's signal (R) is proportional to the number of occupied sites (Aθ), as the analyte's interaction with the surface induces measurable changes in conductance (ΔG), which is normalized via the baseline conductance (G_o).

$$\frac{d^2R}{d\ (A\theta)^2} = 0$$

This relationship holds under specific scenarios, such as doping effects in semiconducting 2D-SnS_2, with the proportionality factor varying based on SnS_2 type and analyte electronegativity. Using a mass action framework, the sensor response rate is derived from the adsorption dynamics, assuming no pre-adsorbed analyte using eq (6.4).

$$\frac{dA\theta}{dt} = k_{ir(ads)}\theta C_a \tag{6.6}$$

Using a variant of an Eley-Rideal-type mechanism, the gas phase species A interacts directly with the empty site in the most basic scenario[Masel, 1996]. Since there is no polymer overlayer on an uncoated array, it is plausible to assume that there is no pre-adsorption isotherm. Applying site balance eq. 6.5

$$\frac{dA\theta}{dt} = k_{ir(ads)}[T\theta - A\theta]C_a \tag{6.7}$$

Solving eq 6.7 for the case of an initially clean array at t = 0:

$$A\theta(t) = (T\theta)(1 - \exp[-k_{ir(ads)}C_a t]$$

$$R(t) = R_{max}(1 - \exp[-C_a . k_{ir(ads)} . t]) \qquad (6.8)$$

Where R_{max} is the maximum response change when sensor is saturated, C_a is the gas concentration, $k_{ir(ads)}$ is the forward rate constant, t is time taken by sensor to reach the response at saturation.

6.5.2. Transient response cycles with fitting curve of Pristine SnS_2 flakes

The experimental transient response curves of SnS_2 sensors for different concentrations of NO_2 vapor (5 to 50 ppm) at room temperature (RT) and 120 °C, as illustrated in Figures 6.5. As depicted in Figure 6.5, the response of the SnS_2 sensing layer increased exponentially upon exposure to the oxidizing NO_2 gas and reached a steady-state saturation level within seconds for each concentration. The dashed red lines in the figures represent the fitting curves for the respective concentrations, showing excellent agreement with the experimental data, as no significant deviation was observed. Figures 6.5 (a, d), summarize the normalized response change (R_{max}) as a function of time for different NO_2 concentrations at RT and 120 °C. The forward rate constant (($k_{ir(ads)}$) is a critical kinetic parameter to evaluate the sensing performance, particularly for on-site detection applications. According to Equation 6.8, the forward rate constant ($k_{ir(ads)}$) varies with the NO_2 concentration (C_a) and is extracted from the fitting curves of the normalized time-dependent response data in Figure 6.5 (c, f). The values of ($k_{ir(ads)}$) for the examined concentration range (5 to 50 ppm) are listed in Table 6.4, showing that the forward rate constant increases with higher NO_2 concentrations, as expected from the theoretical model.

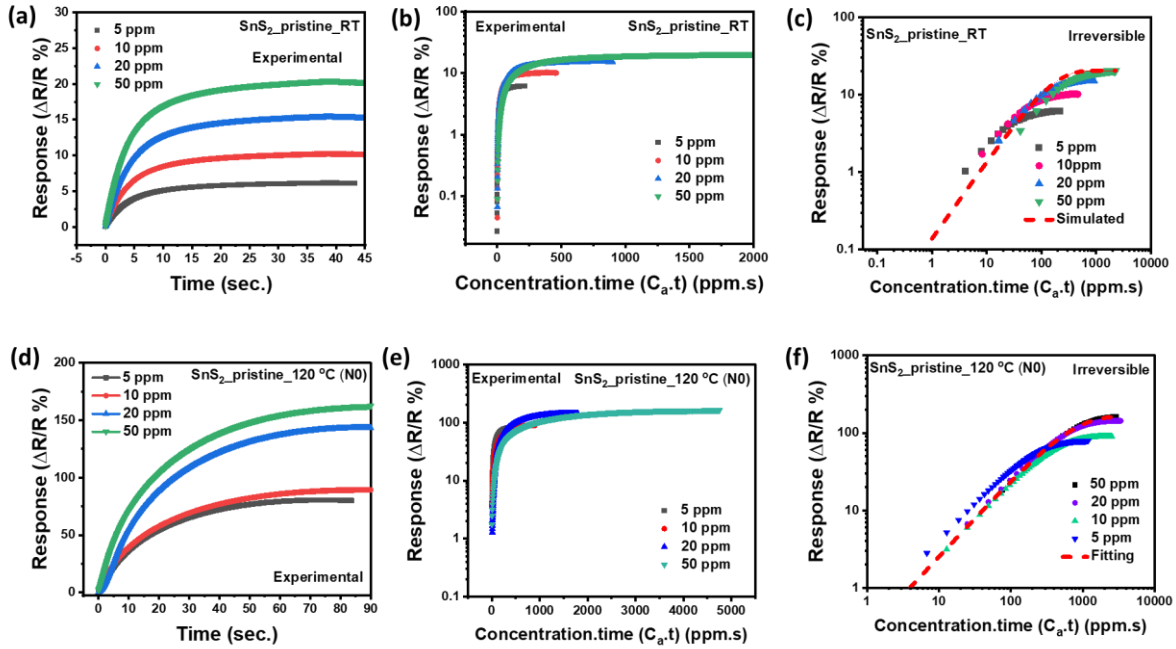


Figure 6.5 Irreversible Adsorption: Experimental (scattered point) and fitted (solid dashed red line) response of VA-SnS_2 based sensor to NO_2 gases for different concentration (5-50ppm) at (a-c) RT, and 120 °C.

6.5.3. Transient response curve with fitting curve of nitrogen plasma treated SnS_2 flakes

We investigate the NO_2 detection on pristine and nitrogen plasma CVD grown on SnS_2 nanoflakes. In our previous paper, the as grown SnS_2 nanoflakes have incomplete recovery and takes longer recovery time due to higher binding affinity and sticking coefficients between the active site of SnS_2 nanoflakes and NO_2. Figure 6.5 (d-f) and Figure 6.6 (e-g), illustrates the transient relative response change parametric for NO_2 concentration of pristine SnS_2 (N0) and Vs_SnS_2 (N12) sample. None attain a stable state, and the surface is renewed using temperature (external

heater) after an arbitrary exposure duration. The corresponding response for NO_2 concentrations of 5, 10, 20, and 50 ppm for N0 and N12 samples were fitted using eq (6.8) and the fitted results are displayed in Figure 6.5 and 6.6. When plotting the relative response against the product, C_at, the graph collapses into one graph, which is an indication of irreversible adsorption (Figure 6.6 (g)). By fitting the response curves of N0, N4, N8, N12 and N16 samples of SnS_2 to eq (6.8), the forward rate constants were determined (Table 6.5). The results revealed that the forward rate constants ($k_{ir(ads)}$) of the N12 sample was 1.39 x 10^{-4} $(ppm.s)^{-1}$, which are 8.93 times higher than the values (1.56 x 10^{-5} $(ppm.s)^{-1}$) of the N0 sample, respectively. As the duration of N_2 plasma was increased and NO_2 was exposed to the sensor, the adsorption rate constants increased till 12 min (N12 sample) and after that it decreased. Table 6.5 shows the forward rate constants ($k_{ir(ads)}$) of pristine and N_2 plasma treated samples toward NO_2 at different concentration of NO_2 gas calculated using irreversible adsorption model. The results revealed that N12 sample exhibited threefold higher adsorption rate constant than other samples, due to the high adsorption energy of NO_2 on the edge site of SnS_2, demonstrating the effect of sulfur vacancies of SnS_2 nanoflakes with abundant edges. In addition, the adsorption rate constant of N16 was decreased compared with N12 due to the formation of N-Sn bond with decreased edge sites, indicating the importance of edge abundant structure for NO_2 sensing.

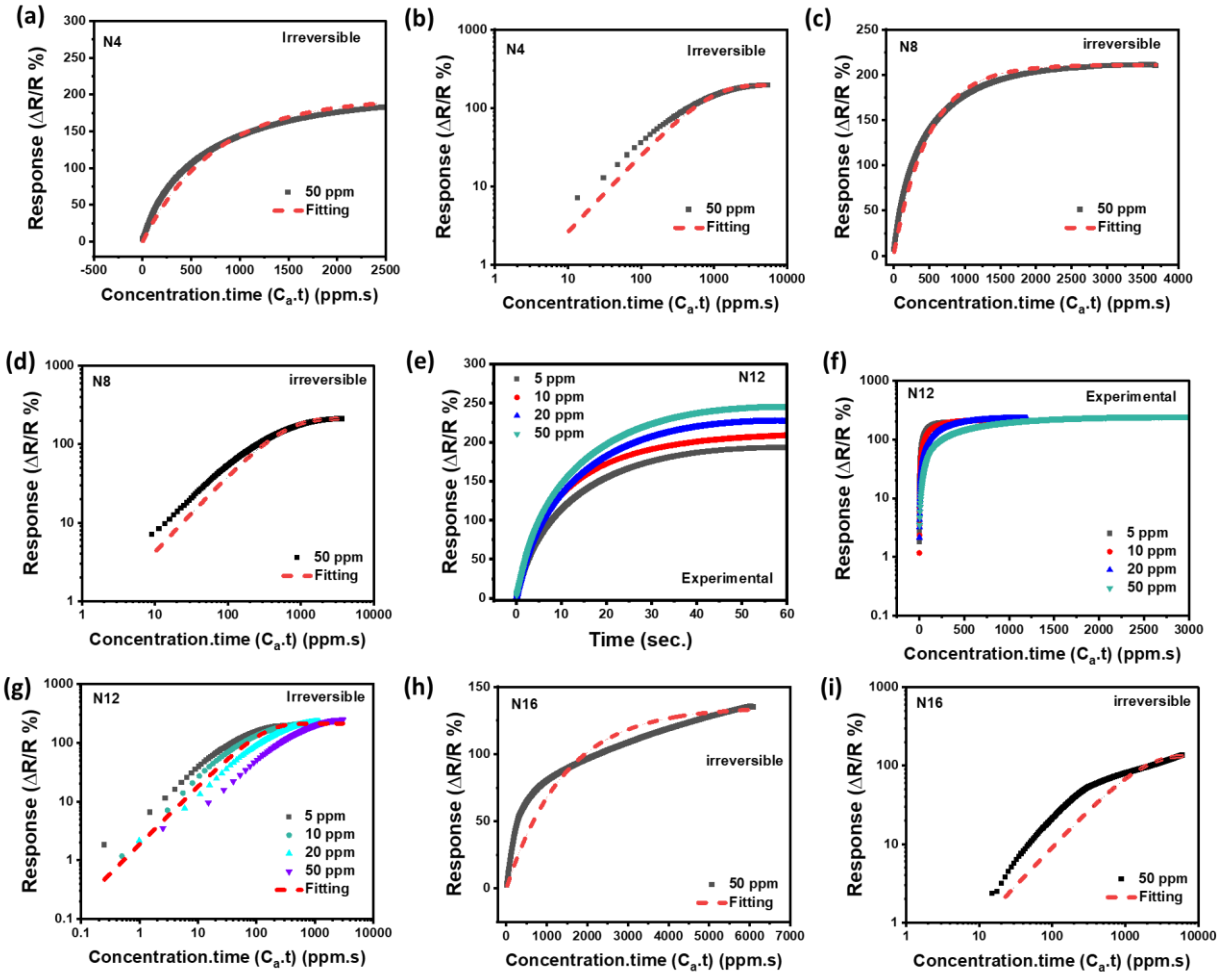


Figure 6.6: Irreversible Adsorption (Nonlinear fit model): Response transients of nitrogen plasma treated SnS_2 (Vs-SnS_2) samples are plotted as a function of (C_at) vs log response the points collapse to a single model operating at 120 °C (a, b) N4 sample, (c, d) N8 sample, (e, f, g) N12 sample, and (h, i) N16 sample, fitted (red color short dashed line), respectively.

Table 6.4: A summary of forward rate ($k_{ir(ads)}$) constant and maximum response of pristine SnS_2 and nitrogen plasma SnS_2 for various concentration of NO_2 at various operating temperatures using irreversible adsorption model.

Sample	Operating Temp.	Gas concentration (PPM)	Maximum value of Response (R_{max})	Forward rate constant ($k_{ir(ads)}$) $(ppm.s)^{-1}$
No	RT	5	6.12	7.45×10^{-3}
		10	10.22	1.85×10^{-3}
		20	15.33	4.62431×10^{-4}
		50	20.42	7.42359×10^{-5}
		Single mode curve fitting	20.42	5.97972×10^{-5}
	120 °C	5	80.50	1×10^{-3}
		10	89.33	2.85493×10^{-5}
		20	143.45	9.58312×10^{-5}
		50	162.66	3.14762×10^{-5}
		Single mode curve fitting	162.66	1.55595×10^{-5}
N12	120 °C	5	192.99	3.49×10^{-3}
		10	208.72	9.52511×10^{-4}
		20	226.45	2.16825×10^{-4}
		50	246.30	3.44613×10^{-5}
		Single mode curve fitting	246.30	1.38979×10^{-4}
N4		50	195.18	2.71037×10^{-5}
N8		50	211.12	4.05085×10^{-5}
N12		50	135.17	1.882×10^{-5}

Table 6.5: Values of various parameter derived by fitting of the response curve as a function of concentration.

Sample	Operating Temperature	Maximum value of Response (R_{max})	Forward rate constant ($k_{ir(ads)}$) $(ppm.s)^{-1}$
No	RT	20.42	5.97972×10^{-5}
No	120 °C	162.66	1.55595×10^{-5}
N4		195.18	2.71037×10^{-5}
N8		211.12	4.05085×10^{-5}
N12		246.30	1.38979×10^{-4}
16		135.17	1.882×10^{-5}

6.6 Summary

In summary, Density functional theory (DFT) calculations were conducted to evaluate the NO_2 gas adsorption properties on three functionalized MoS_2 monolayers: pristine MoS_2, nitrogen-doped MoS_2 (N-MoS_2), and silver-functionalized nitrogen-doped MoS_2 (Ag-N-MoS_2). For pristine MoS_2, weak van der Waals interactions were observed between the surface and NO_2 molecules, with the lowest adsorption energy of -0.53 eV. Nitrogen doping enhanced the adsorption energy to -0.75 eV, with noticeable symmetry breaking in the NO_2 molecule due to unequal bond lengths and a dominant non-bonding interaction between oxygen and nitrogen on the surface ($d_{O\text{-}N(surface)}$ = 2.06 Å). Further functionalization with silver nanoparticles significantly increased the adsorption energy to -1.33 eV. Additionally, SnS_2 monolayers demonstrated a higher NO_2 binding affinity compared to other gases, with an adsorption energy of -1.91 eV, attributed to an increase in carrier concentration upon NO_2 adsorption. DFT studies also revealed that sulfur-vacancy defects on SnS_2 surfaces shifted the adsorption mechanism from physisorption to chemisorption. Among three optimized structures, the highest adsorption energy (2.19 eV) was observed for the structure with one sulfur vacancy, outperforming pristine SnS_2. Using the Lee and Strano reaction mechanism to model gas sensing, it was found that the N12 sample exhibited a higher forward rate constant ($k_{ir(ads)}$ =1.39 x 10^{-4} $(ppm.s)^{-1}$) than NO sample $k_{ir(ads)}$ =1.56 x 10^{-5} $(ppm.s)^{-1}$) at an operating temperature of 120 °C, highlighting the enhanced sensing performance of functionalized materials.